Transient Motion of Circular Elastic Plates Subjected to Impulsive and Moving Loads

By R. S. WEINER

(Manuscript received July 30, 1965)

Forced transient motions of peripherally supported, circular, elastic plates are analyzed according to the classical plate theory. The Green's function for the plate is developed and used to construct solutions for concentrated impulsive loadings, suddenly applied loadings, and moving pressure-wave loadings. The boundary of the plate is considered to be elastically built-in in a manner that prevents transverse edge motion and provides a restoring edge moment linearly related to edge rotation. Thus, limiting cases include a clamped plate and a simply supported plate. Numerical results are included to illustrate the influence of structural and loading parameters on the dynamic response of the plate.

I. INTRODUCTION

During the past decade considerable effort has been channeled toward increasing the capability of equipment to sustain severe nuclear weapon environments. These efforts, commmonly called "hardening," employ various combinations of analytical and experimental approaches, each approach having certain difficulties and shortcomings.

Problems that are analytically tractable are usually restricted to simple and regular geometries and usually incorporate simplifying approximations as to material properties, weapon phenomenon, and separation of the combined weapon effects into independent and separate effects. One of the areas of hardening which lends itself to both analytical and experimental treatment and for which some full-scale nuclear test data are available is the response of structures to an air-blast wave; the analysis of structures subjected to air-blast pressure waves is the subject of the present article. In particular, the transient displacements of circular elastic plates subjected to impulsive and moving loads will be analyzed according to the classical plate theory. The classical, or small

deflection, plate theory does not account for internal structural damping, effects of transverse shear, or rotatory inertia. Consequently, this analysis is strictly applicable when the plate is "thin" (small thickness to radius ratio) and when the higher modes of vibration are of secondary importance;* neglecting internal structural damping results in predicted deflections that are conservative in the sense that they will be larger than corresponding deflections with damping present.

Equations are derived and numerical results are presented for several elemental loadings and for pressure loading waves of constant and decaying magnitude that sweep across the plate with uniform speed. Sweeping pressure-wave loadings occur when the blast wave approaches the plate in other than a face-on direction.

The method of analysis is to construct the Green's function for the plate and then to use principles of superposition in synthesizing solutions for the various loadings of interest.

Previous analyses of circular elastic plate vibrations can be traced to the free vibration analyses of Poisson,[1] and of Kirchhoff,[2] who considered axisymmetric and nonaxisymmetric vibrations respectively. More recent studies of forced vibrations of circular elastic plates include the work of Flynn,[3] Sneddon,[4] Riesman,[5] and the present writer.[6] Mindlin[7] discussed the effects of rotatory inertia and transverse shear deflections on the dynamic plate equation. Elastically restrained plates were investigated by Kantham[8] and by Reid.[9]

II. FORMULATION

2.1 *Equation of Motion*

Forced transverse motions of a homogeneous, isotropic, elastic plate of constant thickness (thickness is restricted to be small in comparison with radius) are governed by the partial differential equation

$$D\nabla^4 w(r,\theta,t) + m\frac{\partial^2 w(r,\theta,t)}{\partial t^2} = p(r,\theta,t) \tag{1}$$

under the restriction that the deflections are small in comparison with the plate thickness, and that the shear deflections, rotatory inertia, and damping can be neglected. Fig. 1 defines the coordinate system and configuration that correspond to (1)

* For a complete discussion of the limitations of the classical plate equation, the reader is referred to Ref. 7.

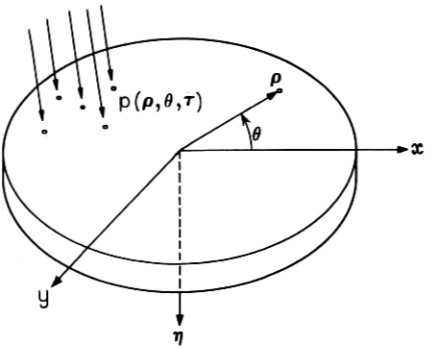

Fig. 1 — Circular plate configuration.

2.2 *Boundary and Initial Conditions*

A plate that is continuous at the origin (non-annular) and elastically built-in* along its periphery has the four boundary (or regularity) conditions:

$$\left.\begin{aligned}
&(a) \qquad w(0,\theta,t) \text{ must be finite} \\
&(b) \qquad \frac{\partial w(0,\theta,t)}{\partial r} \text{ must be finite} \\
&(c) \qquad w(a,\theta,t) = 0 \\
&(d) \qquad -D\left[\frac{\partial^2 w(a,\theta,t)}{\partial r^2} + \frac{\nu}{a}\frac{\partial w(a,\theta,t)}{\partial r}\right] = \beta\frac{\partial w(a,\theta,t)}{\partial r}.
\end{aligned}\right\} \tag{2}$$

Initial conditions that characterize an initially undeflected and stationary plate are

$$w(r,\theta,0) = 0$$

and

$$\frac{\partial w(r,\theta,0)}{\partial t} = 0. \tag{3}$$

These initial conditions are sufficiently general for the applications to

* Elastically built-in edge, as used in this article, refers to a boundary support that prevents transverse edge motion and provides a restoring edge-moment proportional to edge rotation. By properly selecting the constant of proportionality, special cases corresponding to a clamped edge and a simply-supported edge are obtained. A more detailed discussion of this boundary condition appears in Ref. 6.

be considered here; other initial conditions can be treated in a similar manner and will introduce minor changes in the equations developed herein.

III. BASIC SOLUTION

3.1 *Dimensionless System of Equations*

Introducing the dimensionless quantities $\rho \equiv r/a$, $\eta \equiv w/a$, $\tau \equiv t/T$, $\alpha = ma^4/DT^2$, and $\gamma \equiv \nu + (\beta a/D)$, (1) and (2)$d$ become, respectively,

$$\nabla^4\eta(\rho,\theta,\tau) + \alpha \frac{\partial^2\eta(\rho,\theta,\tau)}{\partial\tau^2} = \frac{a^3}{D} p(\rho,\theta,\tau) \tag{4}$$

and

$$\frac{\partial^2\eta(1,\theta,\tau)}{\partial\rho^2} + \gamma \frac{\partial\eta(1,\theta,\tau)}{\partial\rho} = 0. \tag{5}$$

3.2 *Homogeneous Equation*

As a prelude to the solution of (4), the set of eigenfunctions for the plate will be determined. These eigenfunctions are obtained by starting with the homogeneous equation

$$\nabla^4\eta(\rho,\theta,\tau) + \alpha \frac{\partial^2\eta(\rho,\theta,\tau)}{\partial\tau^2} = 0. \tag{6}$$

Separable product solutions of such form that the angular functions and time functions possess the necessary periodicity suggest the following functions:

$$\eta(\rho,\theta,\tau) = R_{nj}(\rho) \begin{Bmatrix} \cos n\theta \\ \text{or} \\ \sin n\theta \end{Bmatrix} e^{i\omega_{nj}\tau}, \tag{7}$$

where $i = \sqrt{-1}$, and n and j are integers.

Substituting (7) into (6) produces an ordinary differential equation in ρ

$$\left(\frac{d^2}{d\rho^2} + \frac{1}{\rho}\frac{d}{d\rho} - \frac{n^2}{\rho^2} + \kappa_{nj}^2\right)\left(\frac{d^2}{d\rho^2} + \frac{1}{\rho}\frac{d}{d\rho} - \frac{n^2}{\rho^2} - \kappa_{nj}^2\right) R_{nj}(\rho) = 0, \tag{8}$$

where

$$\kappa_{nj}^2 = \alpha^{\frac{1}{2}}\omega_{nj}.$$

Equation (8) and the boundary conditions (2) define radial eigenfunctions for the plate.

These radial eigenfunctions are readily found to be

$$R_{nj}(\rho) = I_n(\kappa_{nj})J_n(\kappa_{nj}\rho) - J_n(\kappa_{nj})I_n(\kappa_{nj}\rho), \tag{9}$$

where κ_{nj} is determined from the transcendental equation

$$\frac{2\kappa_{nj}}{1-\gamma} I_n(\kappa_{nj})J_n(\kappa_{nj}) = I_n(\kappa_{nj})J_{n+1}(\kappa_{nj}) + J_n(\kappa_{nj})I_{n+1}(\kappa_{nj}). \tag{10}$$

Two identifying subscripts are associated with κ_{nj} because there is a doubly-infinite set of eigenvalues and eigenfunctions. The first subscript, n, indicates the number of nodal diameters occurring in that mode of vibration and can be any positive integer (representing nonaxisymmetric modes) or zero (representing axisymmetric modes); the second subscript, j, indicates the number of nodal circles (including the boundary circle) and can be any positive integer. Eigenvalues for representative parameters are presented in Table I.

The radial eigenfunction $R_{nj}(\rho)$ as defined by (9) and (10) will be used in the next section as a building block for the development of the Green's function.

3.3 *Green's Function*

Next, the Green's function associated with (4) will be developed. Toward this end, consider the loading function

$$\mathrm{p}(\rho,\theta,\tau) = \frac{1}{\rho_o}\,\delta(\rho-\rho_o)\delta(\theta)\delta(\tau-\tau_o). \tag{11}$$

The solution of (4) with the particular loading function (11) is defined as the Green's function and is denoted by $G(\rho,\theta,\tau;\,\rho_o\,,0,\,\tau_o)$. Without loss of generality, G may be represented by the double series

$$G(\rho,\theta,\tau;\,\rho_o\,,0,\,\tau_o) = \sum_{k=0}^{\infty}\sum_{j=1}^{\infty} R_{kj}(\rho)\cos k\theta\, g_{kj}(\tau), \tag{12}$$

where $g_{kj}(\tau)$ is an unknown function of time that must now be determined.

Introducing (12) into (4), and interchanging the order of differentiation and summation, the result is

$$\sum_k\sum_j \left(\frac{d^2}{d\rho^2}+\frac{1}{\rho}\frac{d}{d\rho}-\frac{k^2}{\rho^2}\right)^2 R_{kj}(\rho)\cos k\theta\, g_{kj}(\tau) + \alpha\sum_k\sum_j R_{kj}(\rho)\cos k\theta\,\ddot{g}_{kj}(\tau) = \frac{a^3}{D}\,\frac{\delta(\rho-\rho_o)\delta(\theta)\delta(\tau-\tau_o)}{\rho_o}. \tag{13}$$

TABLE I — EIGENVALUES FOR CIRCULAR PLATES

n = number of nodal diameters

j = number of nodal circles

j \ n	0	1	2	3	j \ n	0	1	2	3
	$\gamma = 0$					$\gamma = 1.0$			
1	2.1080	3.6744	5.0244	6.2931	1	2.4048	3.8317	5.1356	6.3802
2	5.4188	6.9380	8.3534	9.7044	2	5.5201	7.0156	8.4171	9.7585
3	8.5920	10.188	11.895	13.018	3	8.6568	10.173	11.937	13.042
4	11.747	13.285	15.013	16.214	4	11.792	13.324	15.047	16.238
5	14.896	16.439	18.139	19.397	5	14.931	16.471	18.167	19.418
6	18.043	19.590	21.270	22.569	6	18.071	19.616	21.294	22.588
7	21.187	22.738	24.403	25.734	7	21.212	22.760	24.424	25.752
8	24.331	25.884	27.538	28.895	8	24.352	25.904	27.557	28.911
9	27.475	29.029	30.675	32.052	9	27.493	29.047	30.692	32.067
10	30.618	32.174	33.812	35.207	10	30.635	32.190	33.828	35.220
	$\gamma = 10$					$\gamma = 10^8$			
1	2.9529	4.3001	5.5478	6.7497	1	3.1962	4.6109	5.9057	7.1435
2	5.9280	7.3770	8.7422	10.031	2	6.3064	7.7992	9.1957	10.144
3	8.9762	10.461	12.190	13.158	3	9.4687	10.947	12.694	13.322
4	12.057	13.566	15.265	16.374	4	12.567	14.102	15.813	16.668
5	15.156	16.679	18.358	19.556	5	15.708	17.251	18.939	19.948
6	18.266	19.798	21.463	22.721	6	18.850	20.398	22.069	23.184
7	21.383	22.922	24.576	25.878	7	21.991	23.543	25.202	26.392
8	24.506	26.050	27.695	29.029	8	25.133	26.687	28.336	29.582
9	27.633	29.179	30.818	32.178	9	28.274	29.831	31.472	32.760
10	30.762	32.311	33.943	35.324	10	31.416	32.974	34.609	35.930

Capitalizing on the fact that $R_{kj}(\rho)$ satisfies (8), the first differential operator in (13) can be replaced by ${\kappa_{kj}}^4$ and (13) becomes

$$\sum_k \sum_j [{\kappa_{kj}}^4 g_{kj}(\tau) + \alpha \ddot{g}_{kj}(\tau)] R_{kj}(\rho) \cos k\theta = \frac{a^3}{D} \frac{\delta(\rho - \rho_0)\delta(\theta)\delta(\tau - \tau_0)}{\rho_0}. \tag{14}$$

Next, both sides of (14) are multiplied by

$$\rho R_{lm}(\rho) \cos l\theta \, d\theta d\rho,$$

and integration is performed, first with respect to θ from $0 \to 2\pi$ and then with respect to ρ from $0 \to 1$; by virtue of the orthogonalities (see Appendix), this reduces to

$${\kappa_{lm}}^4 \Theta_{ll} {N_{mm}}^l g_{lm}(\tau) + \alpha \Theta_{ll} {N_{mm}}^l \ddot{g}_{lm}(\tau) = \frac{a^3}{D} R_{lm}(\rho_0)\delta(\tau - \tau_0), \tag{15}$$

where

$$\Theta_{ll} = \begin{cases} \pi & (l \neq 0), \\ 2\pi & (l = 0), \end{cases}$$

and

$${N_{mm}}^l = \tfrac{1}{2}\{{I_l}^2(\kappa_{lm}){J_{l+1}}^2(\kappa_{lm}) - {J_l}^2(\kappa_{lm}){I_{l+1}}^2(\kappa_{lm})\} - \left[\frac{1 + \gamma + 2l}{1 - \gamma}\right] {I_l}^2(\kappa_{lm}){J_l}^2(\kappa_{lm}).$$

For the prescribed initial conditions, the solution of (15) is

$$g_{kj}(\tau) = \frac{a^3}{D} \frac{1}{\alpha} \frac{R_{kj}(\rho_0)}{\Theta_{kk} {N_{jj}}^k} \frac{\sin \omega_{kj}(\tau - \tau_0)}{\omega_{kj}} 1(\tau - \tau_0). \tag{16}$$

Equation (16), when used in conjunction with (12) is the Green's function for the circular elastic plate. Physically, it is the response due to a transverse point impulse applied to the plate.

3.4 *Generalized Green's Function*

The Green's function given by (12) was developed for the case of an impulsive loading singularity located on the line $\theta = 0$. Later, need will arise for the response due to a loading singularity located at the point $(\rho_0, -\alpha_0)$ (see Fig. 2). Employing the trigonometric identity,

$$\cos (A + B) = \cos A \cos B - \sin A \sin B,$$

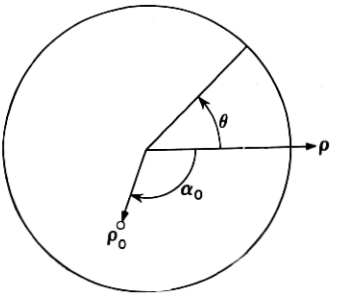

Fig. 2 — Plate coordinate system.

a trivial change of variables produces the corresponding generalized Green's function $G(\rho,\theta,\tau;\ \rho_o\ ,\ \alpha_o\ ,\ \tau_o)$

$$G(\rho,\theta,\tau;\ \rho_o\ ,\ \alpha_o\ ,\ \tau_o) = \sum_{k=0}^{\infty}\sum_{j=1}^{\infty} R_{kj}(\rho)\cos k\alpha_o \cos k\theta\ g_{kj}(\tau) - \sum_{k=1}^{\infty}\sum_{j=1}^{\infty} R_{kj}(\rho)\sin k\alpha_o \sin k\theta\ g_{kj}(\tau). \tag{17}$$

IV. APPLICATION OF GREEN'S FUNCTION

The Green's function as given by (17) will now be utilized to construct solutions for several loadings of technical interest and of practical concern.

4.1 *Ring Loading*

The first example is that of an impulsive concentrated ring pressure distribution given by

$$p(\rho,\theta,\tau) = p(\rho_o)\frac{\delta(\rho-\rho_o)\delta(\tau-\tau_o)}{\rho_o} \tag{18}$$

(see Fig. 3). Physically, this loading corresponds to a concentrated ring impulsive loading applied at radius ρ_o and at time τ_o. A differential element on the ring has a force per unit length $p(\rho_o)/\rho_o$. The resultant displacement of the plate is obtained by superposing contributions due to all of the elements on the ring. This superposition is expressed mathematically by the integral

$$\eta(\rho,\theta,\tau) = \int_0^{2\pi} G(\rho,\theta,\tau;\ \rho_o\ ,\ \alpha_o\ ,\ \tau_o)p(\rho_o)d\alpha_o\ , \tag{19}$$

where α_o is defined by Fig. 3.

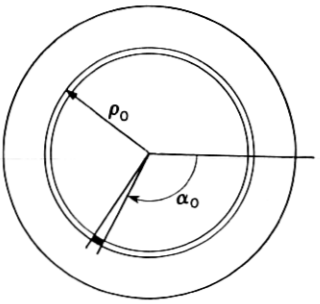

Fig. 3 — Ring loading.

The evaluation of (19) may be simplified considerably by observing that for $l \neq 0$ the integrals are all zero, leaving only the $l = 0$ terms. Accordingly, (19) simplifies to

$$\eta(\rho,\theta,\tau) = \frac{a^3 p(\rho_0)}{D\alpha} \sum_{j=1}^{\infty} \frac{R_{0j}(\rho) R_{0j}(\rho_0)}{N_{jj}{}^0 \omega_{0j}} \sin \omega_{0j}(\tau - \tau_0) 1(\tau - \tau_0). \quad (20)$$

Equation (20) may be recognized as the axisymmetric solution that was obtained previously,[6] provided of course that proper account is taken for the change in nomenclature.

4.2 *Concentrated Line Loading*

As a second example, consider a concentrated line impulse loading specified by

$$p(x,y,\tau) = \delta(x - x_0)\delta(\tau - \tau_0), \quad (21)$$

where x and y are cartesian coordinates appropriate for this problem and defined by Fig. 4. Physically, this loading corresponds to an impulsive concentrated line loading applied at position $x = x_0$ and at time $\tau = \tau_0$.

The force per unit length acting on each element of the line loading given by (21) is

$$\delta(\tau - \tau_0).$$

Likewise, the force acting on the plate due to the Green's function singularity located at (x_0, y) is

$$\delta(\tau - \tau_0).$$

It follows that the resultant deflection due to all differential elements of the line loading is expressed by the superposition integral

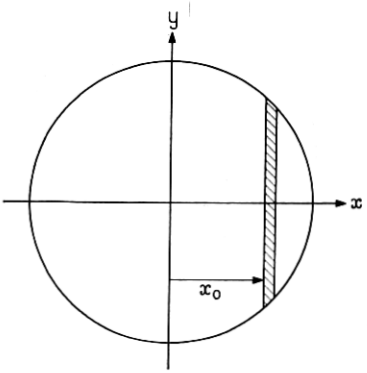

Fig. 4 — Concentrated line loading.

$$\eta(\rho,\theta,\tau;\, x_0\,,\tau_0) = \int_{y=-(1-x_0^2)^{\frac{1}{2}}}^{(1-x_0^2)^{\frac{1}{2}}} G\left(\rho,\theta,\tau;\, [x_0^2 + y^2]^{\frac{1}{2}},\, \tan^{-1}\frac{y}{x_0}\,,\tau_0\right) dy. \quad (22)$$

Substituting (17) into (22) gives the following expression for the dynamic response of the plate:

$$\begin{aligned}
&\eta(\rho,\theta,\tau;\, x_0\,,\tau_0) \\
&= \frac{a^3}{D\alpha}\sum_{l=0}^{\infty}\sum_{m=1}^{\infty}\left[\frac{R_{lm}(\rho)\cos l\theta}{\Theta_{ll}N_{mm}{}^{l}\omega_{lm}}\int_{-(1-x_0^2)^{\frac{1}{2}}}^{(1-x_0^2)^{\frac{1}{2}}} R_{lm}(x_0^2 + y^2)^{\frac{1}{2}}\right. \\
&\quad \cdot\cos\left[l\tan^{-1}\frac{y}{x_0}\right]dy - \frac{R_{lm}(\rho)\sin l\theta}{\Theta_{ll}N_{mm}{}^{l}\omega_{lm}}\int_{-(1-x_0^2)^{\frac{1}{2}}}^{(1-x_0^2)^{\frac{1}{2}}} R_{lm}(x_0^2 + y^2)^{\frac{1}{2}} \\
&\quad \left.\cdot\sin\left[l\tan^{-1}\frac{y}{x_0}\right]dy\right] \times \sin\omega_{lm}(\tau - \tau_0)1(\tau - \tau_0).
\end{aligned} \quad (23)$$

The integrals in (23) are not expressible in closed form; however, they can be integrated numerically. Fortunately, there is one point on the plate where the evaluation does simplify considerably, and that is at the center of the plate, i.e., $\rho = 0$. Restricting our attention to the center of the plate, only the $l = 0$ terms are nonzero, and consequently the center deflection is given by

$$\begin{aligned}
\eta(0,\tau;\, x_0\,,\tau_0) &= \frac{a^3}{\pi\alpha D}\sum_{m=1}^{\infty}\frac{R_{0m}(0)}{N_{mm}{}^{0}\omega_{0m}}\int_0^{(1-x_0^2)^{\frac{1}{2}}} R_{0m}(x_0^2 + y^2)^{\frac{1}{2}}\,dy \\
&\quad \times \sin\omega_{0m}(\tau - \tau_0)1(\tau - \tau_0).
\end{aligned} \quad (24)$$

The integrals in (24) are perfectly well behaved and finite, although they cannot be expressed in closed form. Certain special cases (e.g., for

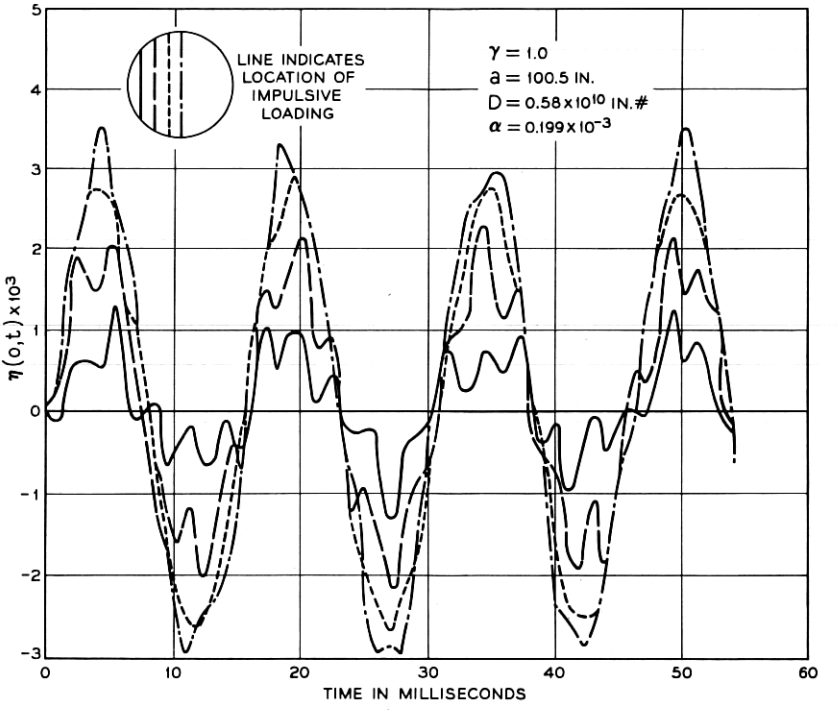

Fig. 5 — Dynamic response due to impulsive line loading ($\gamma = 1.0$).

$x_o = 0$) have been tabulated.[4] Several other cases have been evaluated by the writer, and the results have been incorporated into the numerical examples.

4.3 *Pressure Acting on a Portion of the Plate*

A third example is a plate that is impulsively loaded by a uniform pressure acting on a segment of its surface and unloaded elsewhere. This loading is depicted by Fig. 7.

The center deflection may be thought of as the resultant deflection due to loadings on each line segment from

$$-1 \leqq x_o \leqq x'.$$

A pressure of magnitude $P_o\,\delta(\tau - \tau_o)$ loads each element of width dx_o with a line loading of magnitude $P_o\,\delta(\tau - \tau_o)\,dx_o$. The resultant center deflection is obtained directly from the superposition integral

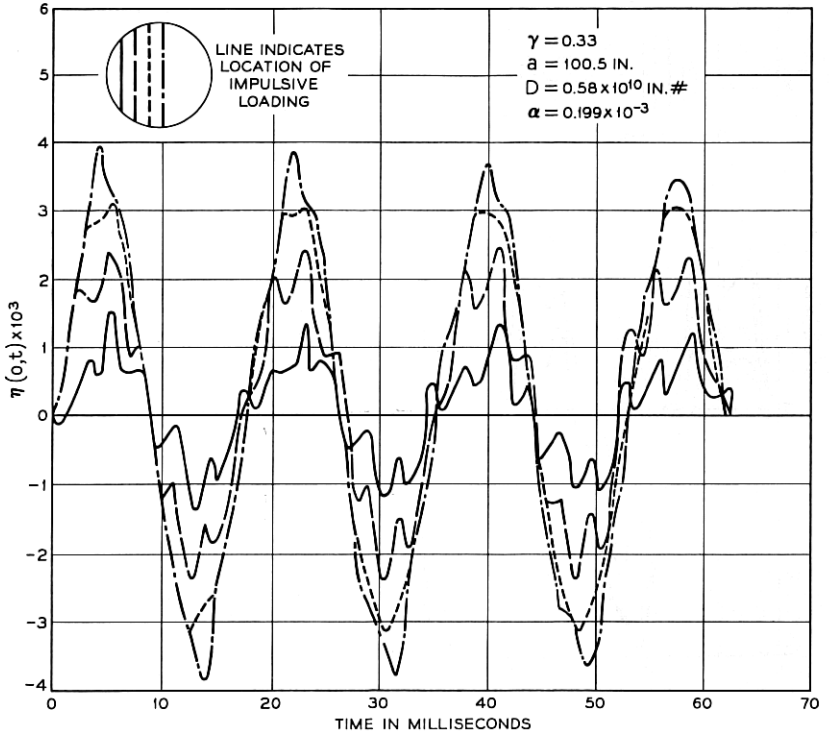

Fig. 6 — Dynamic response due to impulsive line loading ($\gamma = 0.33$).

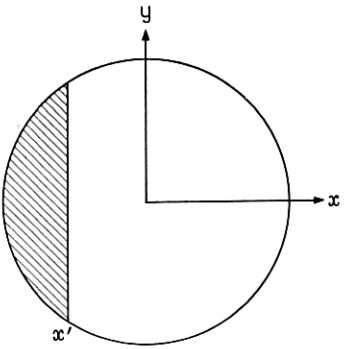

Fig. 7 — Partially loaded plate.

$$\eta(0,\tau;\, x',\tau_0) = \int_{-1}^{x'} P_0\eta(0,\tau;\, x_0,\tau_0)\, dx_0, \tag{25}$$

where $\eta(0,\tau;\, x_0,\, \tau_0)$ is defined in (24).

The integrals in (25) may be integrated numerically. One case that is readily integrable in closed form is when $x' = 1$; that case corresponds to a plate that is suddenly loaded by a uniform pressure over its entire surface. It is readily shown in that instance that (25) reduces to the previously obtained solutions presented in Ref. 6.

If a sector of the plate is loaded with a uniform pressure impulse loading, as indicated by Fig. 8, the superposition methods employed above confirm the intuitive suspicion that the center deflection is the deflection for a uniformly loaded plate multiplied by the quantity $\theta_0/2\pi$, where θ_0 is the included angle of the sector (expressed in radians).

4.4 *Sweeping Pressure Wave*

Next, consider the case of a circular plate loaded by a step blast wave that sweeps across its surface with constant velocity c (expressed in plate diameters per dedimensionalized time) as indicated in Fig. 9. The sector of the plate behind the wave front is loaded by pressure P_0, whereas that portion ahead of the wave front is as yet unloaded.

It is convenient to consider the plate to be divided into strips of equal width Δx_0, with the strips numbered successively from the left hand edge ($x_0 = -1$). This is depicted in Fig. 10.

The first strip is then loaded by a step pressure wave (unloaded until $\tau_0 = 0$) and then loaded with pressure P_0 for $\tau_0 > 0$). After an increment

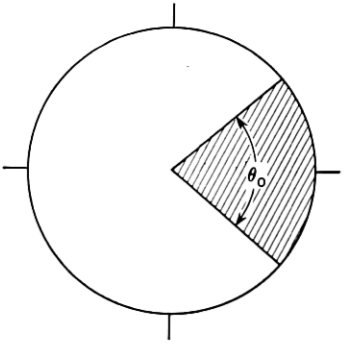

Fig. 8 — Plate loaded on sector.

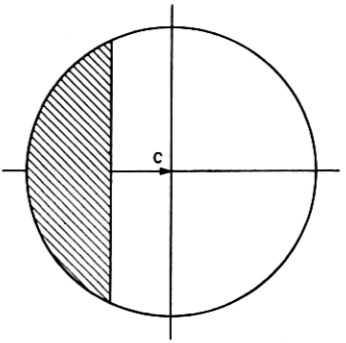

Fig. 9 — Sweeping pressure wave with velocity c.

of time $\Delta\tau_0$ has elapsed, the second strip is loaded by the same step pressure wave (unloaded until $\tau_0 = \Delta\tau_0$ and then loaded with pressure P_0 for $\tau_0 > \Delta\tau_0$). After time interval $2\Delta\tau_0$, the next strip is loaded by the same step pressure loading, and so on, until eventually all strips are loaded by pressure P_0. As the width of the strip is reduced to an infinitesimal, and correspondingly the number of strips increases to infinity, the continuously sweeping pressure wave results.

The solution for a suddenly applied *step* line loading is obtained by integrating (23) with respect to τ_0 (Duhamel integral). The suddenly applied step line loading, denoted by $\bar{\eta}(\rho,\theta,\tau; x_0, \tau_0)$, is given by

$$\bar{\eta}(\rho,\theta,\tau; x_0, \tau_0) = \int_{\tau_0}^{\tau} \eta(\rho,\theta,\tau; x_0, \tau_0)\, d\tau_0 .$$

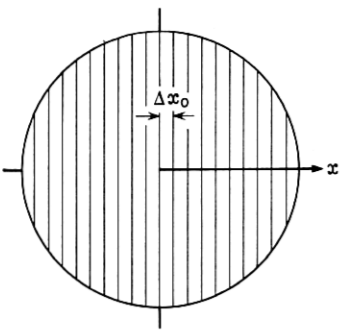

Fig. 10 — Sweeping pressure wave.

The result of this integration is

$$\begin{aligned}\bar{\eta}(\rho,\theta,\tau;x_0,\tau_0) &= \frac{a^3}{D\alpha}\sum_{l=0}^{\infty}\sum_{m=1}^{\infty}\left[\frac{R_{lm}(\rho)\cos l\theta}{\Theta_{ll}N_{mm}{}^{l}\omega_{lm}{}^{2}}\int_{-(1-x_0{}^2)^{\frac{1}{2}}}^{(1-x_0{}^2)^{\frac{1}{2}}} R_{lm}(x_0{}^2+y^2)^{\frac{1}{2}}\right.\\ &\cdot\cos\left[l\tan^{-1}\frac{y}{x_0}\right]dy - \frac{R_{lm}(\rho)\sin l\theta}{\Theta_{ll}N_{mm}{}^{l}\omega_{lm}{}^{2}}\int_{-(1-x_0{}^2)^{\frac{1}{2}}}^{(1-x_0{}^2)^{\frac{1}{2}}} R_{lm}(x_0{}^2+y^2)^{\frac{1}{2}}\\ &\left.\cdot\sin\left[l\tan^{-1}\frac{y}{x_0}\right]dy\right]\times[1-\cos\omega_{lm}(\tau-\tau_0)]1(\tau-\tau_0).\end{aligned} \tag{26}$$

In terms of the solution for the suddenly applied step line loading, the sweeping step wave solution, as obtained by superposition is

$$\eta^*(\rho,\theta,\tau;\,c) = \lim_{\Delta x_0\to 0}\sum_{n=0}^{N} P_0\bar{\eta}\left(\rho,\theta,\tau;-1+n\Delta x_0,\frac{n\Delta x_0}{c}\right)\Delta x_0, \tag{27}$$

$$\text{for}\quad 0\leqq\tau\leqq\frac{2}{c}$$

where $\bar{\eta}$ is given by (26), and η^* is the deflection due to the sweeping wave. In the limit, (27) is expressed by the integral

$$\eta^*(\rho,\theta,\tau;\,c) = P_0\int_{y_0=-1}^{x'}\bar{\eta}\left(\rho,\theta,\tau;\,y_0,\frac{1+y_0}{c}\right)dy_0 \qquad 0\leqq\tau\leqq\frac{2}{c}. \tag{28}$$

Although (28) cannot be evaluated in closed form, (27) is perfectly well suited for numerical evaluation (see Figs. 11, 12, 13), and the ac-

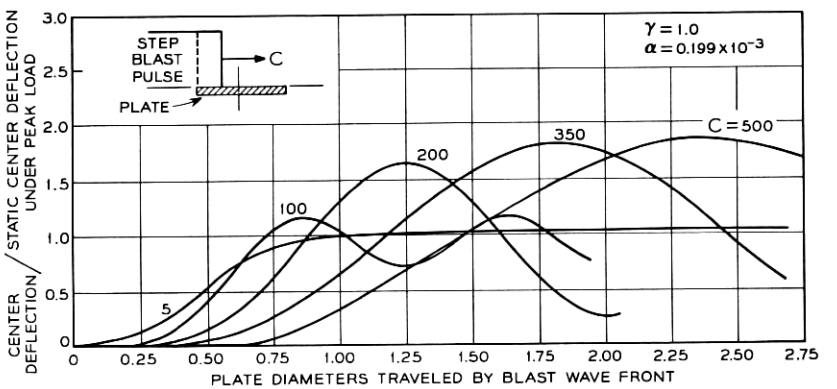

Fig. 11 — Dynamic response due to sweeping step wave ($\gamma = 1.0$).

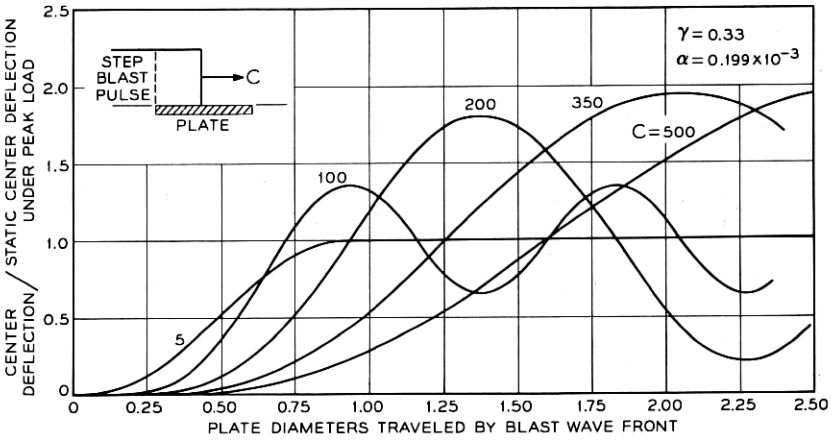

Fig. 12 — Dynamic response due to sweeping step wave ($\gamma = 0.33$).

curacy obtainable is limited only by the computer time expenses associated with the numerical integrations. In the numerical evaluations included in this article, certain symmetry properties were exploited to minimize computer time requirements.

4.5 *Sweeping Pressure Wave with Decay*

As a final example, the case of a sweeping pressure pulse will be considered where the magnitude of the pressure at any point behind the wavefront decays exponentially as a function of the distance behind the

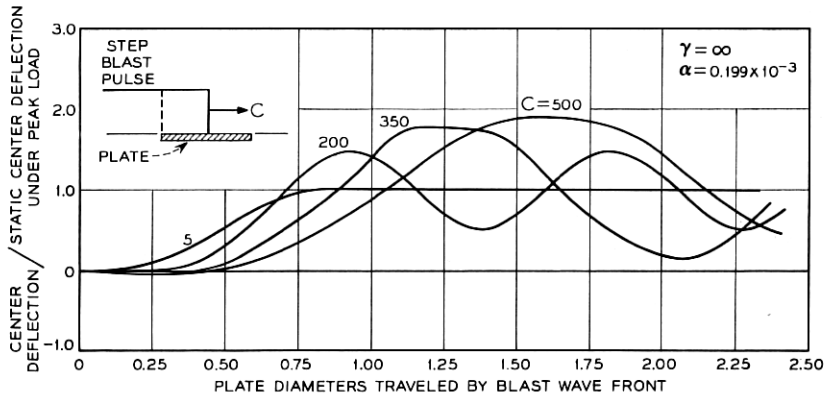

Fig. 13 — Dynamic response due to sweeping step wave ($\gamma = \infty$).

wavefront. As in the previous example, the speed of the pressure wave is considered to be constant.

Referring to Fig. 14, a point at $x = x_0$ is unloaded until time $\tau = (1 + x_0)/c$, at which time the pulse arrives, loading it with pressure P_0. Because of the decay of the loading pulse, the point at x_0 is loaded with pressure

$$P(x_0, \tau) = P_0 \exp\left\{\frac{c}{2} \ln \delta\left[\tau - \frac{1 + x_0}{c}\right]\right\} 1\left(\tau - \frac{1 + x_0}{c}\right). \quad (29)$$

The expressions for the deflection due to the loading given by (29) are identical to (27) and (28) with the exception that $\bar{\eta}$ must be modified. The necessary modification is to replace the factor $[1 - \cos \omega_{lm}(\tau - \tau_0)]$ that appears in (26) by the corresponding factor

$$\frac{\omega_{lm}^2}{\omega_{lm}^2 + (\ln \delta)^2}\left\{\exp\left[\ln \delta(\tau - \tau_0)\right] - \frac{\ln \delta}{\omega_{lm}} \sin \omega_{lm}(\tau - \tau_0) - \cos \omega_{lm}(\tau - \tau_0)\right\}. \quad (30)$$

It can be seen that for the case of zero decay ($\ln \delta = 0$) (30) reduces to the step loading solution (Figs. 15, 16, 17).

V. RESULTS

Dynamic response curves are presented in this article for line impulse loadings and for sweeping waves of both constant and time-diminishing pressure pulses. Figs. 5 and 6 illustrate that a line impulsive loading applied near the diameter excites primarily the first mode of vibration; line loadings applied away from the diameter excite a larger percentage of the higher modes, although as one should expect, the magnitude of the deflection diminishes as the line loading is applied nearer to the edge.

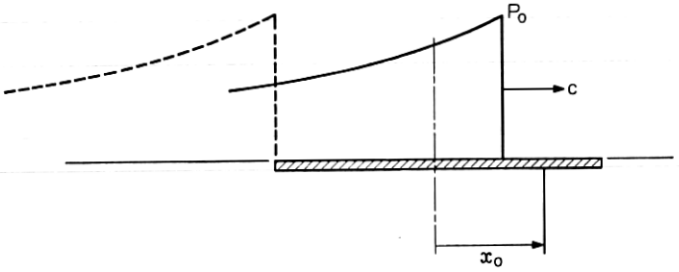

Fig. 14 — Sweeping pressure wave with decay.

functions were computed. In this appendix, corresponding orthogonality properties and normalizing factors will be explored for the non-axisymmetric modes of vibration.

The eigenfunctions,

$$R_{nj}(\rho)\begin{Bmatrix}\cos n\theta \\ \text{or} \\ \sin n\theta\end{Bmatrix} = \{I_n(\kappa_{nj})J_n(\kappa_{nj}\rho) - J_n(\kappa_{nj})I_n(\kappa_{nj}\rho)\}\begin{Bmatrix}\cos n\theta \\ \text{or} \\ \sin n\theta\end{Bmatrix},$$

where $n = 0,1,2, \cdots$ and κ_{nj} satisfies the transcendental equation

$$\frac{2k_{nj}}{1-\gamma} I_n(\kappa_{nj})J_n(\kappa_{nj}) = I_n(\kappa_{nj})J_{n+1}(\kappa_{nj}) + J_n(\kappa_{nj})I_{n+1}(\kappa_{nj}),$$

are solutions to the partial differential equation (6) and satisfy the boundary conditions.

A.1 *Orthogonality*

To begin, recall the well known[10] results

$$\int_0^{2\pi} \cos n\theta \sin m\theta d\theta = 0 \qquad m,n \text{ any integers;}$$

$$\int_0^{2\pi} \cos n\theta \cos m\theta d\theta = \begin{cases} 0 & (n \neq m), \\ \pi & (n = m \neq 0), \\ 2\pi & (n = m = 0); \end{cases}$$

$$\int_0^{2\pi} \sin n\theta \sin m\theta d\theta = \begin{cases} 0 & (n \neq m), \\ \pi & (n = m). \end{cases}$$

These orthogonality relationships imply, in our case, that there is *no coupling* between modes of vibration having n nodal diameters and those modes having m nodal diameters, where $n \neq m$. Thus, one need only concern oneself with relationships such as

$$\int_0^1 \rho R_{nj}(\kappa_{nj}\rho)R_{nk}(\kappa_{nk}\rho)\, d\rho.$$

Therefore, consider the ordinary differential equations (8) that R_{nj} and R_{nk} must satisfy

$$\left(\frac{d^2}{d\rho^2} + \frac{1}{\rho}\frac{d}{d\rho} - \frac{n^2}{\rho^2}\right)^2 R_{nj} = \kappa_{nj}{}^4 R_{nj}$$

and

$$\left(\frac{d^2}{d\rho^2} + \frac{1}{\rho}\frac{d}{d\rho} - \frac{n^2}{\rho^2}\right)^2 R_{nk} = \kappa_{nk}{}^4 R_{nk}.$$

Multiplying the first equation by $\rho R_{nk}d\rho$, and the second by $\rho R_{nj}d\rho$, subtracting, and integrating with respect to ρ from $0 \to 1$ gives

$$\begin{aligned}(\kappa_{nj}{}^4 - \kappa_{nk}{}^4)\int_0^1 \rho R_{nj}R_{nk}d\rho = &\int_0^1 \rho R_{nk}\left(\frac{d^2}{d\rho^2} + \frac{1}{\rho}\frac{d}{d\rho} - \frac{n^2}{\rho^2}\right)^2 R_{nj}d\rho \\ &- \int_0^1 \rho R_{nj}\left(\frac{d^2}{d\rho^2} + \frac{1}{\rho}\frac{d}{d\rho} - \frac{n^2}{\rho^2}\right)^2 R_{nk}d\rho.\end{aligned} \tag{32}$$

The right side of (32) is expanded, and integrated by parts. The lengthy, but routine details of this operation are suppressed in the interest of brevity; the result is

$$\begin{aligned}&\int_0^1 \rho R_{nj}R_{nk}d\rho \\ &= \frac{R_{nk}\left\{\rho\frac{d^3R_{nj}}{d\rho^3} + \frac{d^2R_{nj}}{d\rho^2} - \frac{1}{\rho}\frac{dR_{nj}}{d\rho}\right\} - R_{nj}\left\{\rho\frac{d^3R_{nk}}{d\rho^3} + \frac{d^2R_{nk}}{d\rho^2} - \frac{1}{\rho}\frac{dR_{nk}}{d\rho}\right\}}{(\kappa_{nj}{}^4 - \kappa_{nk}{}^4)} \\ &\quad + \left\{\rho\frac{dR_{nj}}{d\rho}\frac{d^2R_{nk}}{d\rho^2} - \rho\frac{dR_{nk}}{d\rho}\frac{d^2R_{nj}}{d\rho^2}\right\} + \frac{2n^2}{\rho}\left\{\frac{dR_{nk}}{d\rho}R_{nj} - \frac{dR_{nj}}{d\rho}R_{nk}\right\}\Bigg|_0^1.\end{aligned} \tag{33}$$

For the case of $n = 0$,(33) was shown to vanish in Ref. 6 for $j \neq k$. For $n = 1,2, \cdots$ similar reasoning demonstrates that each of the terms in (33) either vanishes or the terms mutually annihilate each other, so that the eigenfunctions are orthogonal under the rather general boundary conditions given in (2).

A.2 *Normalizing Factor*

For $n = 0,1,2, \cdots$, but where $j = k$, both numerator *and* denominator of (33) are zero. Thus, a limiting process must be employed to find the value of

$$N_{jj}{}^n \equiv \int_0^1 \rho R_{nj}{}^2(\rho)d\rho$$

from (33). Differentiating numerator and denominator of (33) with respect to κ_{nk} and then setting $\kappa_{nk} = \kappa_{nj}$, the result is

$$\begin{aligned}N_{jj}{}^n = &\tfrac{1}{2}\{I_n{}^2(\kappa_{nj})J_{n+1}{}^2(\kappa_{nj}) - J_n{}^2(\kappa_{nj})I_{n+1}{}^2(\kappa_{nj})\} \\ &- \frac{1 + \gamma + 2n}{1 - \gamma} I_n{}^2(\kappa_{nj})J_n{}^2(\kappa_{nj}).\end{aligned} \tag{34}$$

This normalizing factor is identical to the axisymmetric normalizing factor derived in Ref. 6 for the axisymmetric case ($n = 0$). An alternative way to derive (34), which was used to check this equation, is to perform the indicated integration directly.

NOMENCLATURE

a	radius of boundary of plate
c	speed at which pressure wave sweeps across plate (expressed in plate diameters per dimensionless time unit)
D	flexural rigidity of plate $\left(\equiv \frac{Eh^3}{12(1-\nu^2)}\right)$
E	Young's modulus
G	Green's function
$g_{kj}(\tau)$	function of time defined by (10)
h	plate thickness
$J_n(z), I_n(z)$	nth order Bessel function and modified Bessel function of argument z
m	mass per unit projected area of plate
$N_{jj}{}^n$	normalizing factor for radial functions, defined by (34)
$p(\rho,\theta,\tau)$	pressure loading on plate
P_o	pressure of loading pulse (constant)
$R_{nj}(\rho)$	radial eigenfunction defined by (7)
r	radial coordinate
t	time
T	time duration used to de-dimensionalize the time variables (chosen for convenience)
w	plate deflection
x,y	cartesian coordinates
α	dimensionless parameter ($\equiv ma^4/DT^2$)
β	modulus of spring on edge of plate
γ	edge-fixity parameter $\left(\equiv \nu + \frac{\beta a}{D}\right)$
δ	decay rate of sweeping pressure pulse
$\delta(z)$	Dirac delta function of argument z
η	dimensionless plate deflection ($\equiv w/a$)
θ	angular coordinate
Θ_{ll}	normalizing factor for angular normal functions
κ_{nj}	eigenvalue corresponding to mode with n nodal diameters and j nodal circles

ν Poisson's ratio

ρ dimensionless radial coordinate ($\equiv r/a$)

τ dimensionless time variable ($\equiv t/T$)

ω_{nj} dimensionless angular frequency associated with the $n-j$ mode of vibration

∇^2 Laplacian operator $\left(\equiv \dfrac{\partial^2}{\partial\rho^2} + \dfrac{1}{\rho}\dfrac{\partial}{\partial\rho} + \dfrac{1}{\rho^2}\dfrac{\partial^2}{\partial\theta^2}\right)$

$1(z)$ unit step function of argument z

Differentiation with respect to time is denoted by dots.

REFERENCES

1. Poisson, S. D., Sur le Mouvement des Corps Elastiques Memoires de l'Academic Royale des Sciences de l'Institut de France, *8,* 1829, pp. 357–370.
2. Kirchoff, G., Uber das Gleichkewicht und die Bewegung einer Elastischen Scheibe, Journal für die reine und angewandte Mathematik (Crelle), *40,* 1850, p. 51.
3. Flynn, P. D., Elastic Response of Simple Structures to Pulse Loadings, Ballistic Research Laboratories Memorandum, Report No. 525, November, 1950.
4. Sneddon, I. N., *Fourier Transforms,* McGraw-Hill Book Company, Inc., New York, N. Y., 1st Ed., 1951, pp. 150–153.
5. Reismann, H., Forced Vibrations of a Circular Plate, Trans. ASME, J. Appl. Mech., *26,* Series E, n. 4, 1959, pp. 526–27.
6. Weiner, R. S., Forced Axisymmetric Motions of Circular Elastic Plates, J. of Appl. Mech., Paper No. 65-APMW-7.
7. Mindlin, R. D., Influence of Rotatory Inertia and Shear on Flexural Motions of Isotropic Elastic Plates, J. of Appl. Mech., *18;* Trans. ASME, *73,* 1951, pp. 31–38.
8. Kantham, C. L., Bending and Vibration of Elastically Restrained Circular Plates, J. Franklin Institute, *265,* June, 1958, pp. 483–91.
9. Reid, W. P., Free Vibrations of a Circular Plate, U. S. Naval Ordnance Laboratory Report 61-186, ASTIA No. 279140, January, 1962.
10. Churchill, R. V., *Fourier Series and Boundary Value Problems,* McGraw-Hill Book Company, Inc., New York, N. Y., 1941, pp. 53–4.